International Journal of Biological Macromolecules 182 (2021) 2037–2047

Contents lists available at ScienceDirect

International Journal of Biological Macromolecules

journal homepage: www.elsevier.com/locate/ijbiomac

# Development of sponge-like cellulose colorimetric swab immobilized with anthocyanin from red-cabbage for sweat monitoring

Salhah D. Al-Qahtani [a], Omer A. Azher [b], Rasha Felaly [c], Abdu Subaihi [d], J. Alkabli [e], Omaymah Alaysuy [f], Nashwa M. El-Metwaly [c,g,*]

[a] Department of Chemistry, College of Science, Princess Nourah Bint Abdulrahman University, Riyadh, Saudi Arabia
[b] Department of Laboratory Medicine, Faculty of Applied Biomedical Sciences, Al-Baha University, Saudi Arabia
[c] Department of Chemistry, Faculty of Applied Science, Umm-Al-Qura University, Makkah, Saudi Arabia
[d] Department of Chemistry, University College in Al-Qunfudah, Umm-Al-Qura University, Saudi Arabia
[e] Department of Chemistry, College of Science and Arts-Alkamil, University of Jeddah, Jeddah, 23218, Saudi Arabia
[f] Department of Chemistry, College of Science, University of Tabuk, Saudi Arabia
[g] Department of Chemistry, Faculty of Science, Mansoura University, El-Gomhoria Street, Egypt

ARTICLE INFO

*Keywords:*
Cellulose
Anthocyanin
Smart aerogel
Sweat
Colorimetric
Biosensor

ABSTRACT

Novel sponge-like biochromic swab was developed *via* immobilization of natural anthocyanin (Cy) biomolecular probe into microporous cellulose aerogel. The current biosensor is characterized with simple preparation, environmentally-friendly, biocompatibility, biodegradability, flexibility, portability and reversibility. This biochromic sponge-like aerogel detector displayed a color change from pink to green-yellow in response to the biochemical changes occurs to sweat. This could be ascribed to intramolecular charge transfer occurs to the molecular system of Cy. Thus, the anthocyanin probe displayed colorimetric variations in UV–Vis absorption spectra *via* a blue shifting from 620 to 529 nm when raising the pH value of the prepared mimic sweat solution. Natural pH sensitive anthocyanin spectroscopic probe was extracted from red-cabbage plant, characterized by HPLC, and encapsulated into microporous cellulose. The microporous sponge-like cellulose swab was prepared by activating wood pulp utilizing phosphoric acid, and then subjected to freeze-drying. This anthocyanin probe is highly soluble in water. Thus, it was encapsulated as a direct dye into cellulose substrate during the freeze-drying process. To allow a better fixation of this water-soluble anthocyanin probe to the cellulose substrate, potash alum was added to the freeze-dried mixture to act as a fixing agent or mordant (M) generating Cy/M coordination complex. The produced Cy/M nanoparticles (NPs) were explored by transmission electron microscopy (TEM). The morphological features of the generated aerogels were investigated by scan electron microscope (SEM), energy-dispersive X-ray (EDX) spectra, and Fourier-transform infrared spectra (FT-IR). The cytotoxicity of the prepared aerogel-based biosensor was also evaluated. The naked-eye colorimetric changes were studied by exploring color strength, UV–Vis spectra and CIE Lab colorimetric coordinates.

## 1. Introduction

Cellulose with a considerably decreased level of crystallinity can be generated either by mechanical disintegration or by subjecting cellulose to a chemical reaction with a mineral acid [1–3]. In comparison to native and regenerated cellulose, cellulose with lower crystallinity has demonstrated an improved dispensability in aqueous solutions due to the increment in surface area. Additionally, the less crystalline cellulose exhibits a better compatibility with other materials, such as lipid, protein and starch [4–6]. The less crystalline cellulose has been useful in the development of sponge-like products. There are different available techniques that have been used to activate cellulose fibers, such as dissolution in 4-methylmorpholine-4-oxide and ionic liquids [1]. Phosphoric acid has been used as an effective recyclable solvent for regenerating cellulose nanowhiskers. Numerous studies have been explored to demonstrate that cellulose has the ability to swell quickly in a concentrated solution of phosphoric acid, and can be dissolved with increasing the temperature [7,8]. During the swelling process of cellulose, phosphoric acid has demonstrated considerably higher hydrolysis rate compared to other strong acids. It can exchange different types of

* Corresponding author at: Department of Chemistry, Faculty of Science, Mansoura University, El-Gomhoria Street, Egypt.
*E-mail address:* nmmohamed@uqu.edu.sa (N.M. El-Metwaly).

https://doi.org/10.1016/j.ijbiomac.2021.05.201
Received 7 April 2021; Received in revised form 27 May 2021; Accepted 30 May 2021
Available online 2 June 2021

cellulose into a highly fibrillated cellulose surface with a high thermal stability [7,8]. Microfibrillated cellulose is a biomaterial distinguished with highly porous scaffolds, low density, non-cytotoxicity, low cost, biocompatibility, large surface area, good swelling capacity, high absorbency, and high strength to weight ratio. Moreover, a variety of active substances can be integrated into different cellulose-derived substrates. Therefore, more investigations were explored toward the development of porous materials, such as aerogels, from the well-known natural, biodegradable and renewable cellulose [9]. Microfibrillated cellulose has been used in various promising applications, such as foodstuffs, personal care, packaging and paper industries. It has been used in the production of filtration systems because of its fine network fibrillated architecture, which is ideal to trap dust particles. It has been also applied in the production of environmental remediation as an adsorbent material to assist in oil spill accidents [10–12]. The development of porous cellulose matrix necessitates an appropriate method to evaporate water to avoid the capillary pressure-stimulated stress, and therefore prevent collapsing the porous system. There have been two major methods that have been employed to remove solvents, including ice-sublimation and supercritical-drying. The ice-sublimation approach in combination with an ice-template is known as cryodesiccation, lyophilization, freeze-casting or freeze-drying [13,14]. It is a freezing process followed with sublimation of solvent, which is a common method to provide cellulose aerogel of low density. The rapid freezing of solvent results in segregating solvent and dispersed phases generating the ice-template. Sublimating the produced ice by the freeze-dry process stops the formation of a liquid-vapor interfaces. This in turn prevents the creation of a capillary pressure to avoid the collapse or deformation of the formed pores [15–17].

The actual potential of a chemosensor for real-time sensing of biological liquids, such as sweat, tears, blister, urine, breast milk, bile and blood, have not been efficiently recognized. This could be attributed to the difficulties correlated to collection of sample, calibration and portability of the sensor device, and real-time detection [18,19]. Sweat is a biological fluid excreted by the skin of human body. Thus, the potential detection of its constituents provides significantly valuable information on the individual physiological case. The human body can excrete a total amount of sweat fluid in the range of 300–700 mL/day [20]. Sweat is essentially composed of water (~99%) in addition to small quantities of nitrogenous substances such as urea and amino acids, metallic and nonmetallic ions such as sodium and chlorides, and metabolic products such as pyruvate and lactate. The pH of perspiration fluid excreted from a normal individual is typically between 4.0 and 6.8, while the pH value of a sweat excreted from an abnormal individual is >6.8. The perspiration sample is less probable to cheating; hence, this sample can be maintained for a longer time period [21,22]. In the case of drug exam, the sweat fluid may contain a quantifiable percentage of opioids such as cocaine, gamma hydroxybutyrates, amphetamines, buprenorphine and cannabinoids. Those opioids typically affect on the pH of a sweat fluid to a higher pH values. Thus, sweat may exhibit significant impacts in forensic science toxicology [23]. There have been some factors that associate the sweat pH value to man health. Examination of a perspiration solution has been used to monitor different health problems, such as cystic fibrosis. The *onsite* sensing of sweat provides a significant approach for collecting rich data on dehydration [24]. In additional, the real-time monitoring of sweat is highly valuable to recognize the health disorders correlated to the changes in the total contents of important biological ions and molecules, such as hyponatremia due to the less total amount of sodium ions [25]. This collected data is useful for optimizing the required pathways of re-mineralization and re-hydration. Changes in the pH value of a sweat fluid played an important function in skin diseases, such as irritant contact dermatitis and acne. The alkalosis metabolism stimulated by ingesting sodium bicarbonate results in a higher pH value of both sweat and blood [26]. Furthermore, it was described that pH of a perspiration fluid increases with raising the rate of perspiration excretion. In addition, the pH value of a perspiration fluid was monitored to increase with raising the total content of sodium cations. The dehydration case results in a higher total content of sodium cations, which can be detected employing a sensor device of high selectivity to sodium ions or indirectly by measuring the pH value of sweat [27].

There are a very limited number of detection techniques reported for sweat monitoring, such as electrochemical and chromatography sensors [28,29]. However, those techniques are non-portability, less specific, expensive, slow, requisite of complicated electric or electronic parts, or even necessitate trained employees. However, the diagnostic tools for sweat monitoring necessitate instant answer with specificity, cheapness and fast response to warranty an early warning of health disorders [20]. Lab-on-a-Chip is an important concept for the development of personalized healthcare sensors, which can be applied toward the improvement of various commercial diagnostic tools already existing in the market. There are many technical advantages that are typically rising up when employing the Lab-on-Chip tools, such as simplicity, low cost, and reusability [30,31]. Colorimetric Lab-on-Chip sensors are distinguished by many advantages over other sensing methods, such as simple miniaturization, low cost, as well as unneeded electric and electronic parts, sophisticated instruments or even trained employees [32–34]. However, a typical colorimetric sensor usually requires synthetic chromophores, which are usually toxic and expensive. Anthocyanin dyes are a class of water-soluble natural flavonoids that can be easily extracted from different renewable crops, such as raspberry, purple cauliflower and red-cabbage that can be harnessed without imposing harms to the environment [35]. Anthocyanins have no environmental impacts, which make them so appealing for customers. Additionally, anthocyanins are safe, biodegradability and nontoxic. Thus, they will not cause harms or health problems upon ingestion or use on man skin. They exhibit different colors at different pH values, including pink or red (pH <7), purple (pH = 7), green-yellow (pH > 7) and colorless (very alkaline solutions). They have been used as pH indicators, colorants in foodstuff, antioxidants and anticancer agents [36,37]. Due to their water-solubility, small molecular size, sensitivity and fast responsiveness, anthocyanins can be considered as suitable active detection sites for encapsulation into fibrous cellulose to afford diagnostic assays for monitoring the biochemical changes in sweat. Collecting high quantities of a sweat sample for an *onsite* test has been usually a complicated procedure as the sensing assay must be accomplished using a highly sensitive, non-cytotoxic, real-time, and highly adsorptive assay to achieve practical evaluation of its contents.

Herein, we develop a simple, fast, real-time, cheap and reversible microfibrillated cellulose-based colorimetric diagnostic tool for visual pH monitoring of a sweat fluid. Microfibrillated cellulose of less crystallinity was prepared to offer a spongy aerogel immobilized with the anthocyanin extract. The biochromic properties of the aerogel biosensor depend mainly on the halochromic activity of anthocyanin. The anthocyanin active detection sites immobilized into the biopolymer cellulose matrix can be considered as an environmentally friendly detection biosensor. The pH of a perspiration fluid can be measured by simple swab of man skin to designate a colorimetric shift from pink to greenish-yellow depending on the person physiological case. This colorimetric shift can be attributed to a reversible deprotonation/protonation process, which results in intramolecular charge delocalization. HPLC was utilized to investigate the contents of the red-cabbage extract, while TEM was applied to investigate the mordant-anthocyanin nanoparticles generated as active spectroscopic sites within the aerogel matrix. The colorimetric measurements were investigated by CIE Lab coordinates and UV–Vis absorption spectra. SEM, FT-IR and EDS were applied to investigate the morphologies of the produced solid state microfibrillated cellulose biosensor. The miniaturized microfibrillated cellulose aerogel immobilized with anthocyanin demonstrated highly porous structure, large surface area and good interconnectivity, which is significant and amenable for a variety of sensing applications with highly efficiency. The current green and sustainable colorimetric biosensor can be directly

utilized as a diagnostic wipe by direct contacting with the individual cuticle, which is valuable for different purposes, such as *onsite* drug examination, as well as healthcare monitoring. In addition, the current method presents *onsite* diagnosis which is very significant for driver drug test and other medical purposes.

## 2. Experimental

### 2.1. Materials

Phosphoric acid ($H_3PO_4$), starch and carboxymethyl cellulose (CMC; DS 0.7) were supplied from Sigma-Aldrich. Fresh harvest of red-cabbage plant was collected from the local market, Egypt. It is distinguished with high growth yield, availability and low cost. Anthocyanin (Cy) was isolated from red-cabbage using previous method [38]. Spectroscopic grade of organic solvents were supplied from Sigma-Aldrich. The bleached wood pulp was monitored to contain alpha cellulose (85%), ash (0.089%) and lignin (0.37%). Potassium alum [$KAl(SO_4)_2$] was supplied from Aldrich. Sodium biphosphate ($NaH_2PO_4$), sodium chloride (NaCl), and L-Histidine monohydrate monohydrochloride were purchased from Sigma-Aldrich.

### 2.2. Extraction of anthocyanin

Red-cabbage plant (1200 g) was cut into smaller pieces, scrubbed with NaCl (120 g) for 60 min, and then crushing and macerating in de-ionized water (3.6 L) for 12 h. After filtration, the produced solution was centrifuged at 2200 rpm for 15 min, and finally decanted to afford a purplish extract with a pH of 6.6. To standardize the generated solution, the maximum intensity of UV–Vis absorbance wavelength was measured. The solution was then diluted with distilled water to reach a maximum absorbance intensity of unity. The extracted solution was maintained in a fridge at 4 °C for more studies. The anthocyanin extract was analyzed by Agilent 1100 HPLC (Waldborn, Germany). UV–Vis absorbance spectrum of the produced extract was studied by HP 8453. Shinoda's analysis was utilized to examine the flavonoids character by adding 1 mL of hydrochloric acid, methyl alcohol (2–3 mL) and a bit of Mg strip to the anthocyanin solution (10 mL) to display a reddish color [39].

### 2.3. Preparation of aerogel biosensor

Cellulose was firstly activated by immersing cellulose wood pulp in distilled water for 24 h. The pulp was then subjected to filtration followed by adding phosphoric acid (50% w/v) with stirring for 24 h. The generated pulp was rinsed 5 folds utilizing distilled water to wash out the phosphoric acid residue, and then stored in the wet form at 10 °C. The complete removal of the phosphoric acid residue was achieved by monitoring the pH of distilled water used in the rinsing process to reach a neutral pH value at 7. This phosphorylated active cellulose (5 g) was subjected to disintegration in distilled water (100 mL), and then gelatinized starch (1.25 g) and carboxymethyl cellulose (1.25 g) were added. After stirring for 1 h, the generated mixture was then blended with the anthocyanin extract at a number of proportions, including 0:100, 5:95, 10:90, 15:85, 20:80, 25:75, 30:70 and 35:65 (v/v) of Cy to activated cellulose solution; which are represented by Cy-0, Cy-5, Cy-10, Cy-15, Cy-20, Cy-25, Cy-30 and Cy-35, respectively. Potassium alum (5% w/v) was then added to each solution. The produced suspensions were poured into Petri dishes, placed in a deep-freezer at −80 °C for 12 h, and then freeze-dried at −40 °C for 24 h using 1–2/LD ALPHA PLUS (Martin Christ, Germany) to provide the corresponding spongy microfibrillated cellulose aerogels.

### 2.4. Characterization

#### 2.4.1. Morphological properties

Scan electron microscopic (SEM) analysis was employed to gather the morphologies of the prepared microfibrillated cellulose aerogels utilizing Quanta FEG-250 at 20 kV. The chemical contents were investigated with energy-dispersive X-ray spectroscopy (EDS-TEAM) connected to SEM. Fourier-transform infrared (FT-IR) spectra were utilized to investigate the functional substituents of the prepared microfibrillated cellulose aerogels in the range between 400 and 4000 $cm^{-1}$ employing Shimadzu 8400S FT-IR Spectrophotometer. Both morphological properties and size of the generated Cy/M NPs were studied by transmission electron microscopy (TEM). TEM micrographs of Cy/M NPs were studied by JEOL 1230 (Japan) at 100 kV. To prepare a sample of Cy/mordant nanoparticles for TEM analysis, the aerogel (Cy-25) was rinsed by stirred in distilled water for 30 min, and then centrifuged at 2200 rpm for 15 min. The aerogel was taken out the generated solution, which was homogenized for an hour. The thermal properties of the prepared sponge-like aerogels was evaluated under air atmosphere in the range of ~25–900 °C by thermal gravimetric analyses (TGA) using STA 6000 Perkin Elmer under a heating rate of 10 °C/min and a flowing rate of 50 mL/min. The crystallinity indices (C.I.) were determined using X-ray diffractometer Bruker D-8 Advance (Germany) employing copper (Kα) with a secondary monochromator at 40 mA and 40 kV according to previous procedure [20] using Segal's equation:

$$\text{C.I.} = [I_{002} - I_{\text{am}}]/I_{002}$$

where $I_{\text{am}}$ is baseline intensity of cellulose amorphous fraction at $2\theta = \sim 18^{\circ}$, and $I_{002}$ is maximum intensity of cellulose crystalline lattice at $2\theta = \sim 22^{\circ}$.

#### 2.4.2. Colorimetric measurements

The coloration measurements of the prepared microfibrillated cellulose aerogels were explored by color strength (*K/S*), UV–Vis absorption spectra, and CIE Lab (L*, a* and b*) colorimetric coordinates using Hunter-Lab Ultra-Scan-Pro spectrophotometer (USA). CIE Lab colorimetric system represents colors as three axes numerical magnitudes; where L* is the color axis representing the sample lightness from white (100) to black (0), a* is the colorimetric axis representing the colorimetric ratio from red (+) to green (−), and b* is the color axis representing the colorimetric ratio from yellow (+) to blue (−).

#### 2.4.3. Sensor evaluation

Sweat mimic solution was developed using standard ISO 105 E04 (1989) procedure. A mixture of NaCl (10 g $L^{-1}$), sodium biphosphate (1 g $L^{-1}$), L-Histidine monohydrate monohydrochloride (0.25 g $L^{-1}$) were subjected to dissolution in de-ionized water (1 L). The pH of the formed solution was attuned at several numerical magnitudes, including 4.5, 5.0, 5.5, 6.0, 6.5, 7.0, 7.5, and 8.0, employing aqueous solutions of sodium hydroxide (0.1 N) and ethanoic acid (0.1 N) in distilled water. The prepared sweat mimic fluids were sprayed on the surface of the microfibrillated cellulose aerogel to show an instant color change from pink to greenish-yellow relying on the pH numerical magnitude of the above developed perspiration mimic fluids. The pH numerical value was controlled with ADWA pH meter AD-11. Photos of the microfibrillated cellulose aerogel biosensor were recorded by Canon A710IS camera.

#### 2.4.4. Reversibility test

The prepared sweat mimic fluid (pH = 8.0) was sprayed on the surface of the microfibrillated cellulose aerogel (Cy-25) to display a color shift from pink to green-yellow. The aerogel was then sprayed with the sweat mimic fluid (pH = 4.5) to show a colorimetric shift back to its origin pink colorimetric shade. This process was performed several cycles, while measuring UV–Vis absorption wavelength before and after every cycle using Ultra-Scan-Pro Hunter-Lab spectrophotometer (USA).

#### 2.4.5. In vitro cytotoxicity study

The cytotoxicity of the microfibrillated cellulose aerogels was studied using normal human epithelial cell line under MTT proliferation bioassay [40]. The cytotoxicity % was determined using the equation bellow:

$$\text{Cytotoxicity}\% = \left(\frac{\text{Reading of the sample}}{\text{Reading of negative control}} - 1\right) \times 100$$

## 3. Results and discussion

### 3.1. Preparation of biochromic aerogel

The current approach depends mainly on the development of a readout colorimetric signal that can be detected upon exposure to sweat mimic fluid (pH >7) using the anthocyanin extract as spectroscopic active guest sites and cellulose aerogel as a host sponge-like swab. Anthocyanins have been used as a halochromic class of natural dyes with the capability to generate a variety of colors, including red in extremely acidic media, pink in slightly acidic media, purple at neutral pH value, greenish-yellow in slightly alkaline solutions, and colorless in extremely high alkaline solutions. Fig. 1 displays different colors arising from anthocyanin extract with changing the pH value from 4.5 to 8.0. The anthocyanin chromophore was extracted from plant by cutting the leaves of red-cabbage into smaller parts, scrubbing with table salt, crushing and macerating in de-ionized water to afford the extract as a purple solution. To inspect the anthocyanin extract, a red color was produced upon using Shinoda's analysis method to examine the flavonoid property [39]. UV–Vis absorbance spectrum of the extract demonstrated three absorption bands monitored at 281 and 331 nm as well as 536 nm, which were assigned to flavonoid and phenolic constituents of anthocyanin, respectively [41]. HPLC was employed to investigate the prepared extract to indicate the presence of diverse phenol compounds at different concentrations as shown in Table 1. The extraction of anthocyanin from red-cabbage has been very simple. However, anthocyanins are a class of naturally occurring direct dyes with high water-solubility, which impart them a very low colorfastness to washing. Therefore, potassium alum has been used as mordant to fix anthocyanin onto the cellulose-based aerogel by forming Cy/mordant coordination complex, which agglomerates to generate nanoparticles. In order to generate activated cellulose, cellulose wood pulp was firstly immersed in distilled water, filtered off under vacuum, mixed with phosphoric acid, and finally washed using distilled water. The activated cellulose was disintegrated in distilled water, and then mixed with gelatinized starch, carboxymethyl cellulose, the anthocyanin extract and potassium alum. The generated suspension was drop-casted in Petri dishes, frozen at −80 °C, and finally freeze-dried to provide a sponge-like microfibrillated cellulose aerogel. The current diagnostic biosensor demonstrated a naked-eye color shift from pink to green-yellow after exposing to a sweat mimic solution (pH >7) as displayed in Fig. 2.

**Table 1**
Phenol compounds monitored in anthocyanin extract as recorded by HPLC.

| Compound | Quantity % |
|---|---|
| *P-coumaric acid* | 2.14 |
| Quercetin-7,3′-dimethylether | 3.46 |
| Quercetin | 4.15 |
| Kaempferol | 44.82 |
| Vanillin | 1.25 |
| Rutin | 21.37 |
| Chlorogenic acid | 1.79 |
| Caffeic acid | 0.64 |
| Cinnamic acid | 2.03 |
| Chrysin | 0.81 |
| Acacetin | 0.92 |
| Catechin | 1.36 |
| Gallic acid | 0.78 |
| Ferulic acid | 13.61 |
| Quercetin-7-methylether | 0.87 |


**Fig. 1.** Colors arising from anthocyanin extract at different pH values in the range of 4.5–8.0.

### 3.2. Morphological characteristics

Solid-state colorimetric biosensors are distinguished with simple operation, rapid response, cheapness, practicability, portability and reversibility. Solid-state biosensors can be employed in household as a commercial indicator and in laboratory assays as a portable device. Therefore, it has been a challenge to develop solid chromogenic sensors for *onsite* sweat monitoring. Moreover, the drilling for environmentally-benign biosensors is highly significant. Cellulose materials, such as aerogels, are distinguished with light weight, abundance, large surface area and fibrous porous scaffold. The morphology of the generated Cy/mordant nanoparticles was investigated by TEM, while both morphologies and chemical compositions of the prepared sponge-like microfibrillated cellulose aerogels dyed with anthocyanin at different ratios were studied by FT-IR, SEM and EDX. The majority of naturally occurring colorants exhibits weak affinity to cellulose fibers. The utility of mordant is essential to enhance their affinity by generating a water-insoluble Al(III)/Cy coordinated complex (Scheme 1) [42–45]. Thus, the water-soluble anthocyanins can be easily applied as a direct dyestuff for dyeing the sponge-like microfibrillated cellulose aerogels in the presence of potassium alum to *in situ* create Cy/Al(III) nanoparticles.


**Fig. 2.** Colorimetric shift of biochromic aerogel biosensor from pink to greenish-yellow upon exposure to sweat mimic solution (pH >7). (For interpretation of the references to color in this figure legend, the reader is referred to the web version of this article.)

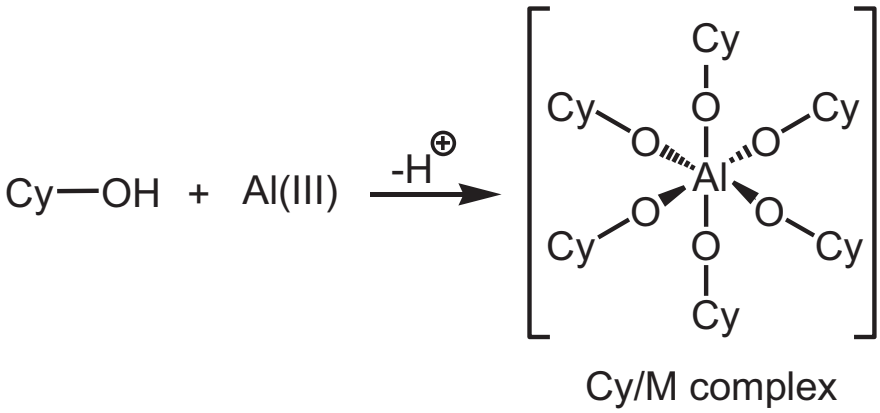


**Scheme 1.** Generation of Cy/Al(III) coordinating complex.

SEM images of Cy-0 and biochromic aerogels integrated with Cy/mordant nanoparticles are shown in Figs. 3 and 4. The particle size of Cy/mordant was determined with Image J software to display diameters of 220–250 nm (Fig. 4). The biochromic Cy/mordant nanoparticles deposited as a film onto the microfibrillated cellulose aerogel can result in a biosensor of high sensitivity. The integration of Cy/mordant nanoparticles into the microfibrillated cellulose aerogel was monitored to influence their porous scaffold to confirm a complete incorporation of Cy/M NPs through the microfibrillated structure. The freeze-drying procedure can offer a tunable porous material with the ability to function as a solid-state sponge-like biosensor swab. Due to increasing porosity and surface area by the freeze-dry process, the generated fibrillated cellulose displayed a higher sensitivity once sprayed with the perspiration mimic solution. Both large surface area and porous character leads to accumulating adsorption onto the aerogel surface and fast diffusion through the mesh. The immobilization of anthocyanin into this three-dimensional microfibrillated cellulose scaffolds results in a potential application toward the development of ultrasensitive biosensors. SEM images displayed morphologies of a sponge-like aerogel as indicated by the open-structured pores. Cellulose fibers were found to aggregate as fibrous bundles owing to the adhesive function induced by starch. The diameters of pores were measured by Image J program connected to SEM. Microfibrillated cellulose fibrous alignment was monitored with a fibrous width of 15–25 μm and a porous diameter of 20–75 μm. The presence of vertical small-width fibrous bundles could be ascribed to the freeze-drying mechanism, which results in the creation of a porous wall with less deformation in the fibrous system. The immobilization of anthocyanin was found to influence the morphologies of the produced aerogels as their surfaces appeared as a coated-like shape owing to the deposited Cy/mordant nanoparticles onto the aerogel surface.

The density of Cy/mordant nanoparticles increased with increasing the ratio of anthocyanin from Cy-5 to Cy-25, which is attributed to increasing the density of the deposited Cy/mordant nanoparticles on the surface of the aerogel. However, the density of Cy/mordant nanoparticles was monitored to decrease again on the surface of the aerogel with increasing the ratio of anthocyanin from Cy-25 to Cy-35, which is attributed to the higher adsorption and diffusion of Cy/mordant nanoparticles inside the bulk of the aerogel [20]. The diffusion of anthocyanin active sites trapped within the aerogel matrix at higher concentrations results in shrinking the porous wall; and therefore, the porous diameter decreases upon raising the total content of anthocyanin. In other words, the distance between cellulose fibers is reduced, which could be attributed to hydrogen bonding between the phenolic anthocyanin and the hydroxyl groups of the microfibrillated cellulose [20]. Therefore, a large density of Cy/M NPs is embedded inside the microfibrillated cellulose bulk. The current biochromic sensor displayed a high sensitivity to the aqueous sweat mimic solution, which can be attributed to the large surface area and highly spongy microfibrillated scaffolds. Thus, better adsorption and diffusion of sweat fluid through this porous microfibrillated matrix to Cy/mordant nanoparticles was monitored. Both EDX diagrams and elemental mapping images of both Cy-0 and biochromic aerogels at three different positions are shown in Fig. 5 and Table 2. The chemical compositions were approximately identical at the three studied spots to confirm a uniform distribution of Cy/M NPs.

Both morphological assembly and particle diameter of Cy/mordant nanoparticles incorporated into the microfibrillated cellulose aerogel were also studied using TEM micrographs to indicate diameters in the range of 220–250 nm as shown in Fig. 6. To generate an aqueous suspension of Cy/M NPs, the biochromic aerogel (Cy-25) was stirred in deionized water, homogenized, and finally filter off under vacuum to afford the corresponding aqueous suspension for TEM analysis.

FT-IR spectroscopy was utilized to inspect the functional substituents of the prepared aerogels as shown in Fig. 7. The major absorption peaks of Cy-0 and aerogels-immobilized with anthocyanin are the vibration peaks of hydroxyl and aliphatic CH. The hydroxyl vibration peak of chromogenic aerogels was detected at 3328 $cm^{-1}$. The stretch peak of

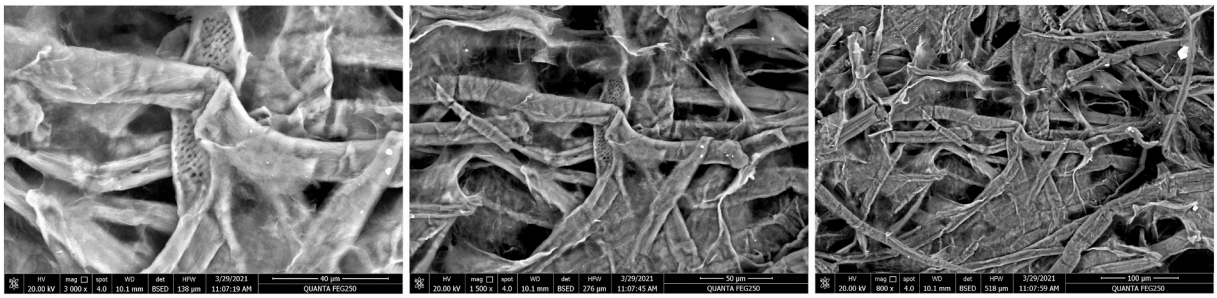

**Fig. 3.** SEM micrographs of Cy-0.

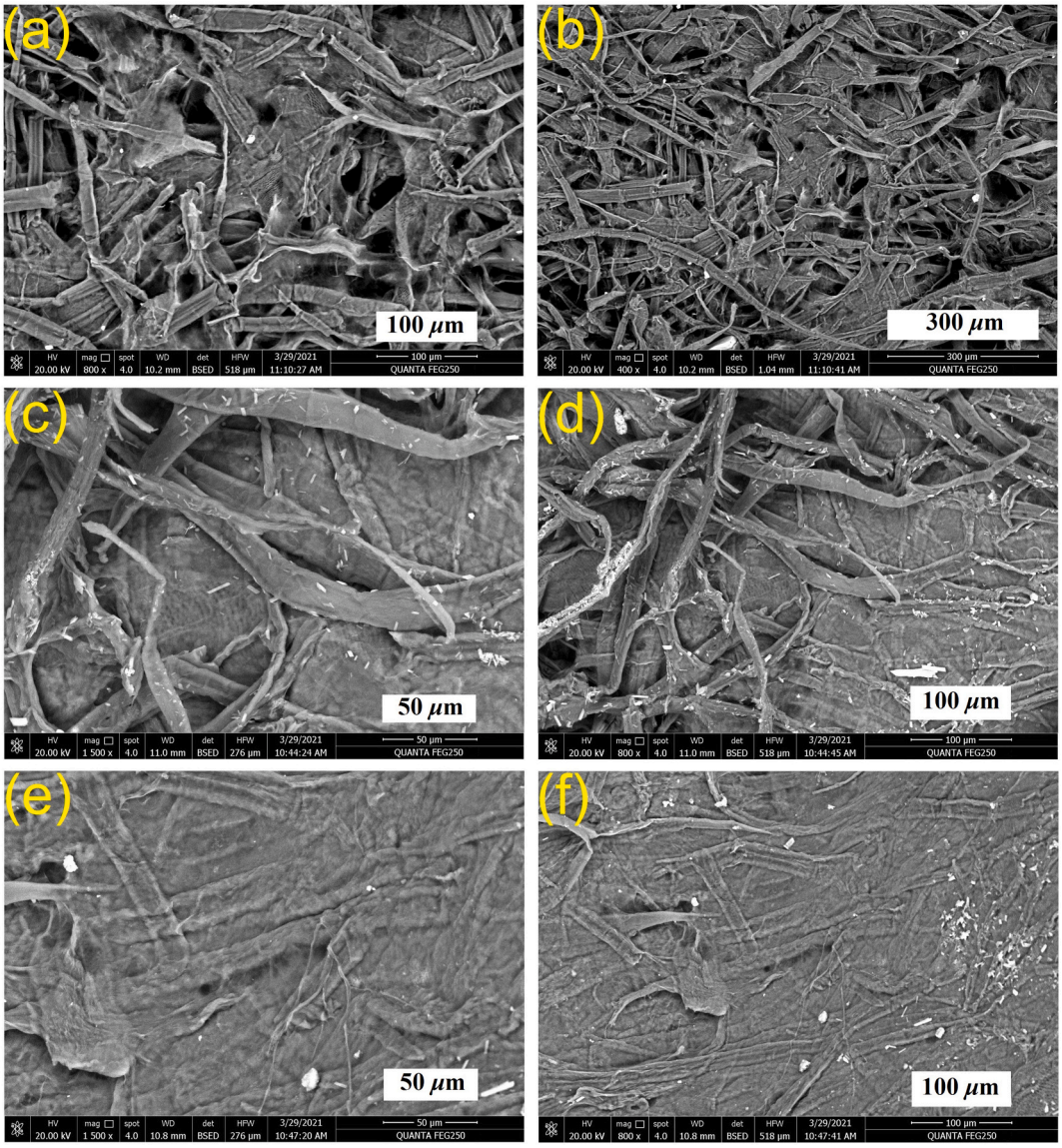


**Fig. 4.** SEM micrographs of biochromic aerogels integrated with Cy/M NPs; Cy-5 (a-b), Cy-25 (c-d), and Cy-35 (e-f).

CH was observed at 2906 $cm^{-1}$. No major shifting was detected in either hydroxyl or aliphatic absorption peaks. The hydroxyl peak intensity at 3328 $cm^{-1}$ was found to decrease in the case of inactive cellulose owing to functionalizing cellulose by phosphorylation at the sixth carbon atom of the glucose unit. The band at 982 $cm^{-1}$ is attributed to l, 4-$\beta$ ether bonding between glucose units was also monitored to decrease upon activating cellulose. This could be attributed to the degradation impact of orthophosphoric acid upon activation. The band observed at 1640 $cm^{-1}$ due to the hydroxyl bend vibrations from moisture molecules. This hydroxyl bending peak intensity decreased with increasing the amount of anthocyanin ratio. Considerable decrease was observed in the intensity of the hydroxyl absorption peak with raising the total content of anthocyanin. This can be attributed to the increased density of the deposited dye onto the surface of the microfibrillated cellulose aerogel, which result in increasing the coordination binding of potassium alum with the hydroxyl substitutes from both of phenol anthocyanin and cellulose. Therefore, a large density of Cy/M NPs is embedded inside the microfibrillated cellulose bulk. No key changes were detected in FT-IR spectra previous and following to exposure to sweat mimic solution.

### 3.3. Crystallinity index

Cellulose is not soluble in aqueous media and common solvents. Hence, it was a requirement to dissolute cellulose using safe and nontoxic solvents, such as orthophosphoric acid. Dissolving cellulose in orthophosphoric acid resulted in breaking the intra and intermolecular H-bonds of polymer chains converting cellulose to simple glucose units. Table 3 displays the crystallinity index (C.I.) values of inactivate and phosphorylated cellulose, and cellulose sponges, including Cy-0 and anthocyanin-immobilized aerogels at the least (Cy-5) and highest (Cy-35) total contents of anthocyanin. Due to activating cellulose with phosphoric acid, the crystallinity index was found to decrease. Thus, more external fibrous surface was accessible leading to an internal cohesion during lyophilization to generate a sponge-like aerogel. The crystallinity index of Cy-0 was found to increase slightly as a result of bringing the fibers nearer to each other throughout the freeze-drying process. Considerable increase in the crystallinity index was monitored upon immobilizing the anthocyanin extract, which was integrated within the fibers surface and matrix. The internal porous wall, within the sponge bulk, was brought nearer to each other leading to further fibrous alignment; and consequently increase C.I. of cellulose fibers. Increasing

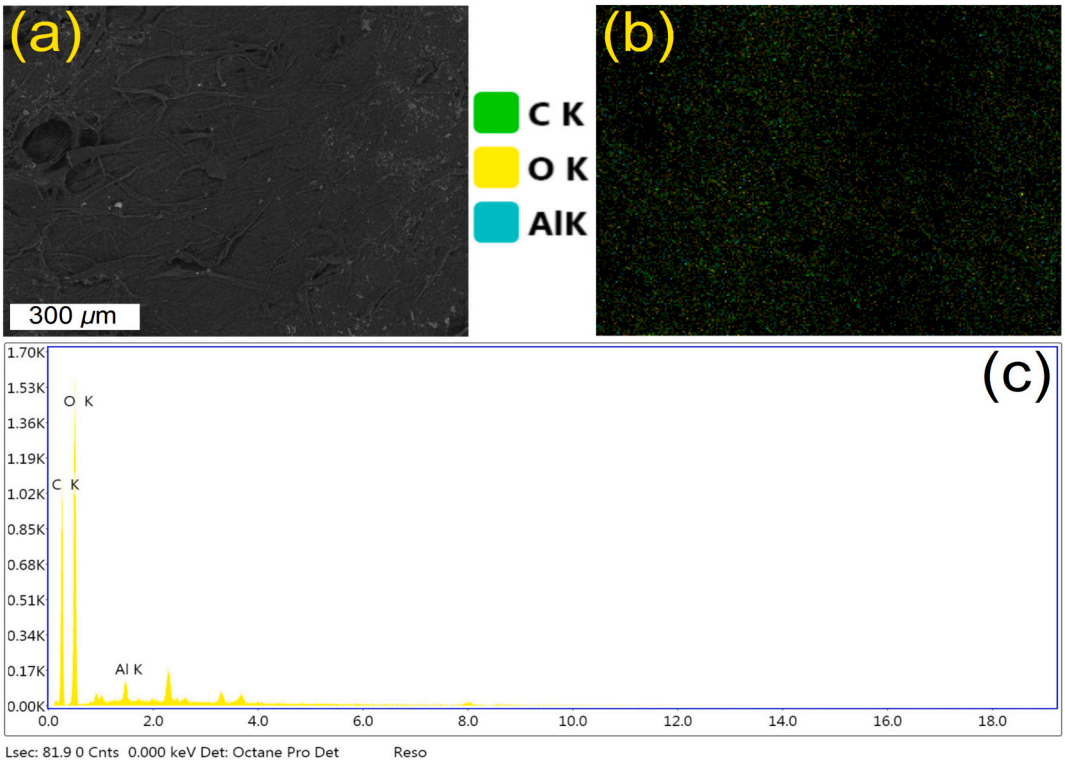


**Fig. 5.** Elements maps (a, b) and EDS diagram (c) of biochromic aerogel immobilized with Cy/mordant; Cy-25.

**Table 2**
Chemical compositions (weight %) of Cy-0 and chromogenic aerogels immobilized with Cy/mordant complex (Cy-25) at three different position (A, B and C) on the aerogel surface.

| Aerogel | | C | O | Al |
|---|---|---|---|---|
| Cy-0 | | 42.63 | 57.37 | 0 |
| Cy-25 | A | 40.69 | 58.08 | 1.23 |
| | B | 40.93 | 57.80 | 1.27 |
| | C | 40.42 | 58.20 | 1.38 |

the ratio of anthocyanin resulted in bringing the fibers further closely to each other; and consequently increases C.I. of cellulose fibers.

### 3.4. Thermal stability

Fig. 8 displays the thermal gravimetric analysis (TGA) of inactivate and phosphorylated cellulose, and cellulose sponges, including the aerogel (Cy-0) and anthocyanin-immobilized aerogels at the lowest (Cy-5) and highest (Cy-35) total contents of anthocyanin. The weight loss of inactivated cellulose fibers was monitored by two major phases. The initial phase was correlated to evaporating the absorbed moisture at 100 °C. The second phase was correlated to degradation of the cellulosic bulk at 345 °C to smaller segments with a residual of about ~18% as a result of carbonization. The bulky step of weight loss from activated cellulose was explained as two sub-steps at 175 and 500 °C. The weight loss of the phosphorylated substrate (weight loss of 24%) was monitored at higher rate compared to inactivated cellulose at the early heating range. The second sub-stage was distinguished with a weight of 66% at 500 °C. The phosphorylated substrate demonstrated less thermal stability than the inactivated one at the initial heating ranges. Nonetheless, the existence of a phosphate functional substituent improved the thermal stability of the phosphorylated substrate at elevated temperatures with a residual of about ~28%, which is more than the residue of

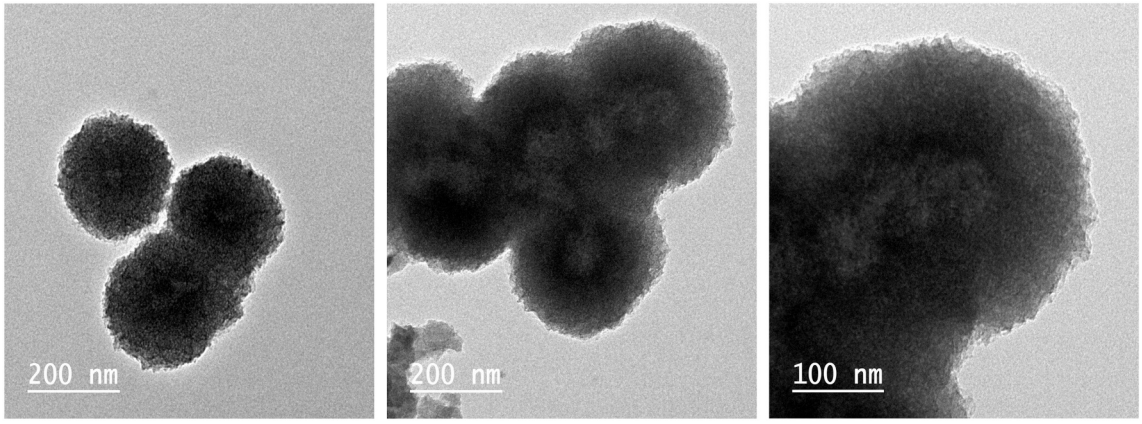


**Fig. 6.** TEM images of Cy/mordant nanoparticles extracted from Cy-25.

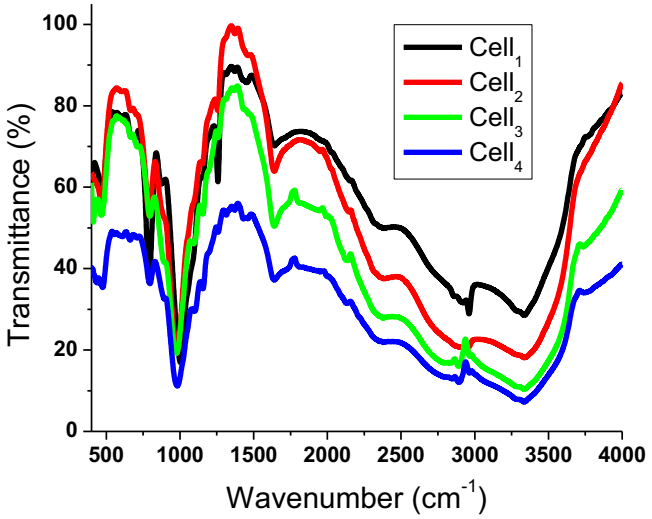


**Fig. 7.** FT-IR spectral analysis of cellulose ($Cell_1$), phosphorylated cellulose ($Cell_2$), and sponges immobilized with anthocyanin Cy-5 ($Cell_3$), and Cy-35 ($Cell_4$).

**Table 3**
Crystallinity index of inactivate and phosphorylated cellulose fibers, and Cy-0, Cy-5 and Cy-35 aerogels.

| Sample | Inactivated cellulose | Activated cellulose | Cy-0 | Cy-5 | Cy-35 |
|---|---|---|---|---|---|
| C.I. | 0.51 | 0.45 | 0.47 | 0.89 | 0.93 |

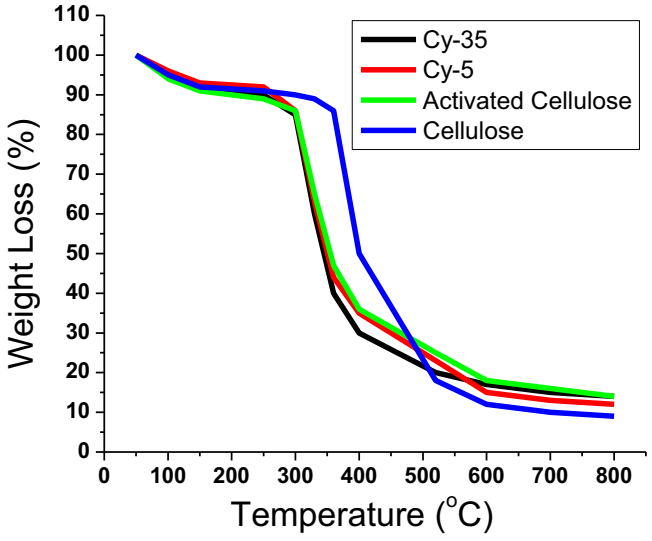


**Fig. 8.** TGA of inactivated cellulose (a), activated cellulose (b), Cy-0 (c), Cy-5 (c), and Cy-35 (c).

inactivated substrate (18%). The blank aerogel (Cy-0) was distinguished with bulky weight loss exchange of 61% at 395 °C because the bulk constitution is phosphorylated substrate. The immobilization of anthocyanin (Cy-5) influenced the bulk weight loss as a slight shift was monitored to lower temperature at 375 °C. The highest total content of anthocyanin (Cy-35) displayed an increased bulky weight loss at 355 °C. Hence, the existence of an organic entity immobilized into cellulose fibers accelerates the rate of pyrolysis.

### 3.5. Cytotoxicity assessment

Because the developed biosensor is wiped directly by man cuticle, the cytotoxic activity of the sponge-like cellulose was evaluated *in vitro* under MTT bioassay. The results demonstrated no cytotoxic effect of the prepared biosensor at the highest ratio of anthocyanin (Table 4).

### 3.6. Colorimetric measurements

The preparation of fibrillated cellulose biopolymer immobilized with a chemical probe biomolecule to provide a biosensor sponge-like swab to examine the biochemical variations that occur in a perspiration fluid is of high significance. This tool can be applied for private healthcare examination. Nonetheless, it has been a difficult practice to gather a sweat sample for real-time analysis to accomplish a practical testing. Herein, we introduce an easy, rapid, portable and sensitive spongy biosensor for sensing perspiration. The biosensor was fabricated from the naturally occurring anthocyanin pH indicator immobilized into microfibrillated cellulose aerogel. To inspect the biosensor, we produce a sweat fluid to act as an imitated perspiration solution, which can be sprayed onto the biochromic aerogel to display an immediate colorimetric change from pink to greenish-yellow relying on the pH numerical magnitude of the perspiration fluid as demonstrated in Fig. 9. The perspiration solution with a pH of 7.0 was investigated in detail. The immediate colorimetric shift of the sponge-like biosensor from pink to greenish-yellow can be easily observed by UV–Vis absorbance spectra (Fig. 10) and naked-eye (Fig. 11).

The quantity of anthocyanins in the chromogenic aerogel demonstrated a major factor in the biochromic properties of this aerogel. No major differences were detected in the color coordinates of the white Cy-0 aerogel due to exposing to the aqueous sweat mimic solutions. On the other side, the exposure of an aerogel immobilized with anthocyanin to an aqueous sweat mimic solution led to a hypsochromic shifting in the absorbance wavelength from 620 to 529 nm (Fig. 10) in association with considerable changes in *K/S* and CIE Lab coordinates. The coloration properties of the biochromic aerogels upon employing various quantities of Cy are summarized in Table 5. The *K/S* was found to increase with increasing the added amount of anthocyanin, which indicates an improved hue between Cy-5 and Cy-25. However, a little increment in *K/S* was detected with raising the quantity of Cy solution between Cy-25 and Cy-35. Thus, the optimum coloration results were monitored for Cy-25. Furthermore, *K/S* was found to increase after exposure to sweat mimic solutions at a pH value higher than 7. The CIE Lab values of the biochromic aerogels displayed significant differences compared to Cy-0. L* considerably decreased to designate darker shade with raising the ratio of the anthocyanin solution between Cy-5 and Cy-25, which could be attributed to increasing the added ratio of Cy. However, little differences in L* were detected with raising the ratio of Cy solution between Cy-25 and Cy-35, This can be attributed to decreasing the added ratio of Cy. Considerable change in L* was detected toward smaller numerical values following to spraying with sweat mimic solution with a pH >7. Previous to exposing to the perspiration mimic solution, decreased negative b* and increased positive a* were detected with the higher ratios of Cy solution to indicate a pink shade. Following to exposure to sweat mimic solution, increased negative a* and increased positive b* numerical magnitudes were detected with the higher ratios of Cy solution to indicate a green-yellow color. Following to spraying with sweat mimic solution, the positive a* was changed to negative

**Table 4**
Cytotoxicity of Cy-35 at 100 μg $mL^{-1}$ under MTT assay.

| Aerogel | $IC_{90}$ (μg $mL^{-1}$) | $IC_{50}$ (μg $mL^{-1}$) | Notes |
|---|---|---|---|
| Cy-35 | – | – | 0 at 100 ppm |
| DMSO | – | – | 0 at 100 ppm |
| Negative control | – | – | 0% |

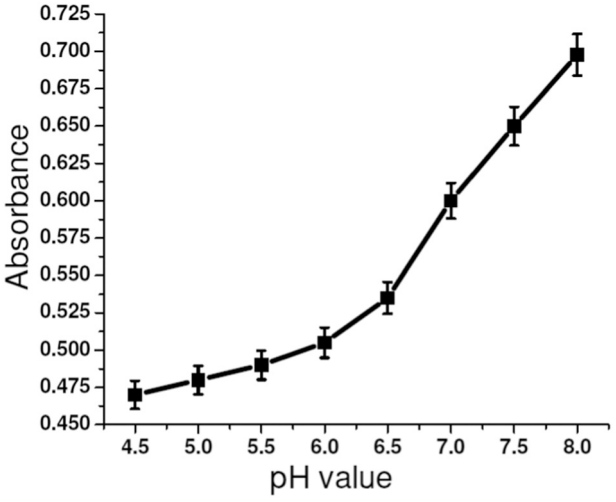


**Fig. 9.** Changes in UV–Vis absorption intensities of Cy-25 at 529 nm upon exposure to different perspiration fluids with different pH values.

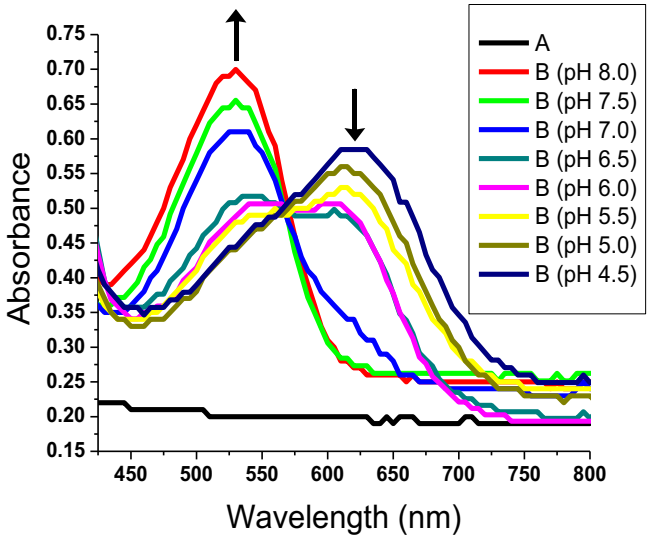


**Fig. 10.** UV–Vis spectral shifts of Cy-0 (A), and Cy-25 (B) with increasing the pH value of the sweat mimic solution to result in a blue shifting from 620 to 529 nm. (For interpretation of the references to color in this figure legend, the reader is referred to the web version of this article.)

numerical magnitudes indicating a colorimetric shift from pink to green-yellow. Similarly, the negative b* was changed to positive numerical magnitudes after spraying with the sweat mimic fluid.

### 3.7. Mechanism of detection

The colorimetric evaluation depends on pH responsiveness of anthocyanin demonstrating a color shift from pink to greenish-yellow on the biochromic aerogel (colorless for an aqueous solution of anhthocyanin) upon exposure to aqueous sweat mimic solution at a pH value higher than 7. Increasing the pH numerical value of the sweat mimic solution to alkaline was translated to a readout naked-eye colorimetric signal due to deprotonation of anthocyanin as depicted in Scheme 2. There are a number of techniques that have been described for sweat monitoring, such as hydrazone-cellulose composite [20], radio-frequency identification sensor [46], laser-ablated microfluidics [47], chromatography [48], and electrochemical methods [49]. However, those methods are expensive, slow, non-portable, hard to operate, non-biodegradable, or even difficult to use. The colorimetric biosensors have been an effective, real-time, inexpensive and simple practice for sweat monitoring. Herein, the natural microporous sponge-like cellulose swab together with the anthocyanin biological molecule verified to be an effective, inexpensive, biodegradable, highly sensitive and non-toxic biosensor for sweat monitoring.

The reversibility of the biosensor (Cy-25) was examined by reversing the maximum absorbance wavelength back and forth between pink at 620 nm (before exposure to perspiration solution) and greenish-yellow at 529 nm (after exposure to perspiration solution). The sponge-like aerogel swab was then left to air-dry for 15 min. The process was carried out numerous times, while recording UV–Vis absorbance wavelength before and after each cycle as shown in Fig. 12. It was obvious that this procedure was highly reversible.

## 4. Conclusions

Colorimetric sponge-like microfibrillated cellulose biosensor was successfully prepared, characterized and assessed for sweat monitoring. The current biochromic device represents a simple and practical method for practical monitoring of perspiration solutions. Anthocyanin-based natural pH indicator extracted from red-cabbage exhibits an ability to increase the intramolecular charge delocalization upon deprotonation in an alkaline medium. Exposure to sweat mimic solutions led to changing the observed color from pink at 620 nm to greenish-yellow at 529 nm relying on the pH numerical magnitude of the perspiration solution. The aerogel biosensor showed a high sensitivity. Morphologies, elemental contents and colorimetric properties were investigated by SEM, FT-IR, EDX, TGA, TEM, HPLC, DSC and CIE Lab colorimetric screening. The particle size of the Cy/mordant coordinative complex deposited into the aerogel was in the range of 220–250 nm. The aerogel matrix displayed porous scaffolds resulting from microfibrillated fibrous alignments demonstrated by a cross-section width of about 15–25 μm and micro-sporous architectures with a pore size in the range of 20–75 μm. Activating cellulose with phosphoric acid improved the dissolution of compact fibrous architectures to result in stable suspension of microfibrillated cellulose fibers, which was freeze-dried leading to the formation of a sponge-like matrix. Unlike cellulose fibers, the produced aerogels displayed an improved thermal stability owing to phosphorous content. The nitrogen-containing organic content immobilized onto cellulose fiber was able to accelerate pyrolysis to result in higher bulky weight loss at 355 °C. The prepared sponge with the high ratio of anthocyanin displayed no cytotoxic activity to man cuticle. The current biosensor is an easy, green and reversible chromic pattern for realistic detection of a perspiration condition using a sponge-like material

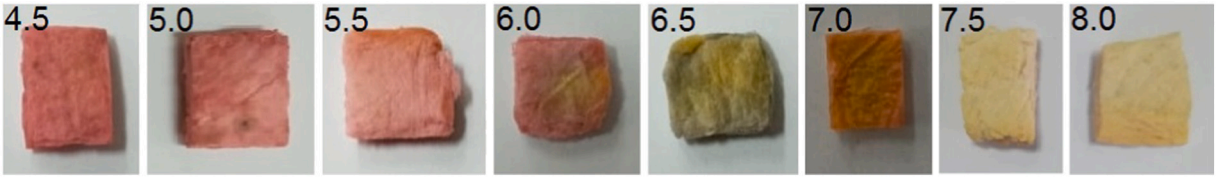


**Fig. 11.** Color change of biochromic aerogel (Cy-25) from pink to greenish-yellow after spraying with sweat mimic solution at different pH values from 4.5 to 8.0. (For interpretation of the references to color in this figure legend, the reader is referred to the web version of this article.)

**Table 5**
Coloration measurements at different ratios of the anthocyanin solution before and after exposure to the sweat mimic solution at a pH value higher than 7.

| Cy (v %) | *K/S* | | L* | | a* | | b* | |
|---|---|---|---|---|---|---|---|---|
| | Before | After | Before | After | Before | After | Before | After |
| Cy-0 | 0.73 | 0.66 | 93.37 | 94.94 | 0.03 | 0.02 | 1.31 | 1.23 |
| Cy-5 | 1.57 | 0.98 | 57.15 | 77.94 | 6.45 | −3.62 | −36.52 | 8.57 |
| Cy-10 | 3.11 | 3.45 | 50.11 | 74.90 | 11.06 | −6.55 | −32.06 | 17.59 |
| Cy-15 | 6.86 | 3.80 | 46.36 | 69.48 | 16.51 | −9.52 | −26.39 | 25.62 |
| Cy-20 | 8.84 | 5.42 | 42.85 | 67.95 | 20.79 | −10.55 | −22.49 | 25.84 |
| Cy-25 | 9.93 | 5.84 | 41.01 | 66.82 | 23.14 | −12.88 | −20.38 | 27.63 |
| Cy-30 | 10.36 | 6.30 | 40.41 | 66.23 | 23.55 | −14.07 | −18.49 | 28.06 |
| Cy-35 | 10.71 | 6.56 | 40.87 | 65.94 | 23.88 | −14.78 | −17.57 | 28.63 |

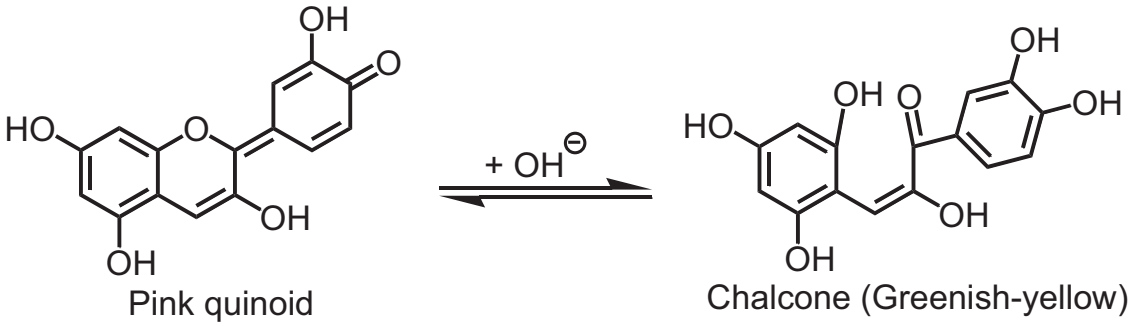


**Scheme 2.** Suggested mechanistic pathway for colorimetric sweat monitoring by anthocyanin.

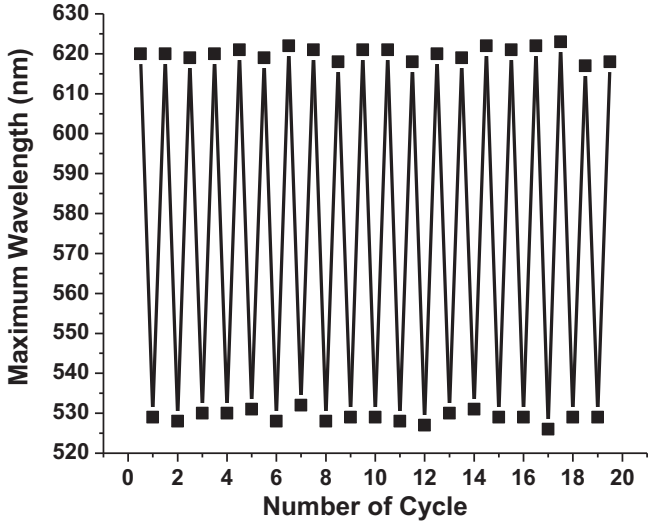


**Fig. 12.** Switching the absorbance wavelength of Cy-25 between 620 and 529 nm.

derived from natural cellulose biopolymer to function as a host holding natural anthocyanin biomolecule for potential drug test. In comparison to formerly described perspiration sensing techniques which typically require complicated electronic constituents, the current colorimetric biosensor is an easy-to-use device for real-time sweat sensing.

## Declaration of competing interest

The authors declare that they have no conflict of interests.

## Acknowledgment

This research was funded by the Deanship of Scientific Research at Princess Nourah Bint Abdulrahman University through the Fast-track Research Funding Program.

## References

[1] Yan Shi, Rui Kong, Fang Yang, Shaowei Ren, Jinglei Xie, Participation of sodium sulfamate as hydrogen bond-donating and hydrogen bond-accepting additive in the dissolution of cellulose in NaOH aqueous solution, Cellulose 25 (5) (2018) 2785–2794.
[2] Bruno Medronho, Björn Lindman, Competing forces during cellulose dissolution: from solvents to mechanisms, Curr. Opin. Colloid Interface Sci. 19 (1) (2014) 32–40.
[3] Mohammad Ghasemi, Marina Tsianou, Paschalis Alexandridis, Assessment of solvents for cellulose dissolution, Bioresour. Technol. 228 (2017) 330–338.
[4] Mohammad Ghasemi, Paschalis Alexandridis, Marina Tsianou, Cellulose dissolution: insights on the contributions of solvent-induced decrystallization and chain disentanglement, Cellulose 24 (2) (2017) 571–590.
[5] Yang-Lei Chen, Xun Zhang, Ting-Ting You, Feng Xu, Deep eutectic solvents (DESs) for cellulose dissolution: a mini-review, Cellulose 26 (1) (2019) 205–213.
[6] Alistair W.T. King, Janne Asikkala, Ilpo Mutikainen, Paula Järvi, Ilkka Kilpeläinen, Distillable acid–base conjugate ionic liquids for cellulose dissolution and processing, Angew. Chem. Int. Ed. 50 (28) (2011) 6301–6305.
[7] Juho Antti Sirviö, Fabrication of regenerated cellulose nanoparticles by mechanical disintegration of cellulose after dissolution and regeneration from a deep eutectic solvent, J. Mater. Chem. A 7 (2) (2019) 755–763.
[8] Dong Tian Qing, Jinguang Hu, Fei Shen, Gang Yang, Yanzong Zhang, Shihuai Deng, Jing Zhang, Yongmei Zeng, Yaodong Hu, Fates of hemicellulose, lignin and cellulose in concentrated phosphoric acid with hydrogen peroxide (PHP) pretreatment, RSC Adv. 8 (23) (2018) 12714–12723.
[9] Mandeep Singh, Vikas Pahal, Dheeraj Ahuja, Isolation and characterization of microfibrillated cellulose and nanofibrillated cellulose with "biomechanical hotspots", Carbohydr. Polym. 234 (2020), 115827.
[10] Alina S. González-Ugarte, Islam Hafez, Mehdi Tajvidi, Characterization and properties of hybrid foams from nanocellulose and kaolin-microfibrillated cellulose composite, Sci. Rep. 10 (1) (2020) 1–12.
[11] Xuejing Zheng, Xiaoxiao Li, Jinyang Li, Liwei Wang, Wenjing Jin, Ying Pei, Keyong Tang, Efficient removal of anionic dye (Congo red) by dialdehyde microfibrillated cellulose/chitosan composite film with significantly improved stability in dye solution, Int. J. Biol. Macromol. 107 (2018) 283–289.
[12] Yuan Li, Huining Xiao, Yuanfeng Pan, Lidong Wang, Novel composite adsorbent consisting of dissolved cellulose fiber/microfibrillated cellulose for dye removal from aqueous solution, ACS Sustain. Chem. Eng. 6 (5) (2018) 6994–7002.
[13] Yajun Huang, Ting Zhou, Song He, Huan Xiao, Huaming Dai, Bihe Yuan, Xianfeng Chen, Xiaobing Yang, Flame-retardant polyvinyl alcohol/cellulose nanofibers hybrid carbon aerogel by freeze drying with ultra-low phosphorus, Appl. Surf. Sci. 497 (2019), 143775.
[14] Hao-Yang Mi, Xin Jing, Alexander L. Politowicz, Edward Chen, Han-Xiong Huang, Lih-Sheng Turng, Highly compressible ultra-light anisotropic cellulose/graphene

aerogel fabricated by bidirectional freeze drying for selective oil absorption, Carbon 132 (2018) 199–209.
[15] Clara Jiménez-Saelices, Bastien Seantier, Bernard Cathala, Yves Grohens, Effect of freeze-drying parameters on the microstructure and thermal insulating properties of nanofibrillated cellulose aerogels, J. Sol-Gel Sci. Technol. 84 (3) (2017) 475–485.
[16] Deniz Ciftci, Ali Ubeyitogullari, Raquel Razzera Huerta, Ozan N. Ciftci, Rolando A. Flores, Marleny D.A. Saldaña, Lupin hull cellulose nanofiber aerogel preparation by supercritical $CO_2$ and freeze drying, J. Supercrit. Fluids 127 (2017) 137–145.
[17] Cong Wang, Zheng-Ze Pan, Wei Lv, Bilu Liu, Jie Wei, Xiaohui Lv, Yi Luo, Hirotomo Nishihara, Quan-Hong Yang, A directional strain sensor based on anisotropic microhoneycomb cellulose nanofiber-carbon nanotube hybrid aerogels prepared by unidirectional freeze drying, Small 15 (14) (2019), 1805363.
[18] Jie Zhao, Hexia Guo, Jinghua Li, Amay J. Bandodkar, John A. Rogers, Body-interfaced chemical sensors for noninvasive monitoring and analysis of biofluids, Trends Chem. 1 (6) (2019) 559–571.
[19] Jessica Schultz, Zakir Uddin, Gurmit Singh, Matiar M.R. Howlader, Glutamate sensing in biofluids: recent advances and research challenges of electrochemical sensors, Analyst 145 (2) (2020) 321–347.
[20] Tawfik A. Khattab, Sawsan Dacrory, Hussein Abou-Yousef, Samir Kamel, Smart microfibrillated cellulose as swab sponge-like aerogel for real-time colorimetric naked-eye sweat monitoring, Talanta 205 (2019), 120166.
[21] Mallika Bariya, Hnin Yin Yin Nyein, Ali Javey, Wearable sweat sensors, Nat. Electron. 1 (3) (2018) 160–171.
[22] Conghui Liu, Tailin Xu, Dongdong Wang, Xueji Zhang, The role of sampling in wearable sweat sensors, Talanta 212 (2020), 120801.
[23] Christopher Legner, Upender Kalwa, Vishal Patel, Austin Chesmore, Santosh Pandey, Sweat sensing in the smart wearables era: towards integrative, multifunctional and body-compliant perspiration analysis, Sensors Actuators A Phys. 296 (2019) 200–221.
[24] Qi Zhang, Xuewei Wang, Vanessa Decker, Mark E. Meyerhoff, Plasticizer-free thin-film sodium-selective optodes inkjet-printed on transparent plastic for sweat analysis, ACS Appl. Mater. Interfaces 12 (23) (2020) 25616–25624.
[25] E. Scarpa, V.M. Mastronardi, F. Guido, L. Algieri, A. Qualtieri, R. Fiammengo, F. Rizzi, M. De Vittorio, Wearable piezoelectric mass sensor based on pH sensitive hydrogels for sweat pH monitoring, Sci. Rep. 10 (1) (2020) 1–10.
[26] Jie Zhao, Hexia Guo, Jinghua Li, Amay J. Bandodkar, John A. Rogers, Body-interfaced chemical sensors for noninvasive monitoring and analysis of biofluids, Trends Chem. 1 (6) (2019) 559–571.
[27] Alicia Zoerner, Susanne Oertel, Michael P.M. Jank, Lothar Frey, Bernd Langenstein, Thomas Bertsch, Human sweat analysis using a portable device based on a screen-printed electrolyte sensor, Electroanalysis 30 (4) (2018) 665–671.
[28] Seung Yun Oh, Soo Yeong Hong, Yu Ra Jeong, Junyeong Yun, Heun Park, Sang Woo Jin, Geumbee Lee, et al., Skin-attachable, stretchable electrochemical sweat sensor for glucose and pH detection, ACS Appl. Mater. Interfaces 10 (16) (2018) 13729–13740.
[29] Marc Parrilla, Inmaculada Ortiz-Gómez, Rocio Canovas, Alfonso Salinas-Castillo, María Cuartero, Gastón A. Crespo, Wearable potentiometric ion patch for on-body electrolyte monitoring in sweat: toward a validation strategy to ensure physiological relevance, Anal. Chem. 91 (13) (2019) 8644–8651.
[30] Bidhan Chandra Dhar, Nae Yoon Lee, Lab-on-a-chip technology for environmental monitoring of microorganisms, Biochip J. 12 (3) (2018) 173–183.
[31] Nongnoot Wongkaew, Marcel Simsek, Christian Griesche, Antje J. Baeumner, Functional nanomaterials and nanostructures enhancing electrochemical biosensors and lab-on-a-chip performances: recent progress, applications, and future perspective, Chem. Rev. 119 (1) (2018) 120–194.
[32] Samir Kamel, Tawfik A Khattab, Recent advances in cellulose-based biosensors for medical diagnosis, Biosensors 10 (6) (2020) 67.
[33] Hasan Aldewachi, Tamim Chalati, M.N. Woodroofe, Neil Bricklebank, B. Sharrack, Philip Gardiner, Gold nanoparticle-based colorimetric biosensors, Nanoscale 10 (1) (2018) 18–33.
[34] Yoojin Choi, Ji Hyeon Hwang, Sang Yup Lee, Recent trends in nanomaterials-based colorimetric detection of pathogenic bacteria and viruses, Small Methods 2 (4) (2018), 1700351.
[35] Bambang Kuswandi, Ni P.N. Asih, Dwi K. Pratoko, Nia Kristiningrum, Mehran Moradi, Edible pH sensor based on immobilized red cabbage anthocyanins into bacterial cellulose membrane for intelligent food packaging, Packag. Technol. Sci. 33 (8) (2020) 321–332.
[36] Giovanni Agati, Kamel Soudani, Lorenza Tuccio, Elisa Fierini, Naïma Ben Ghozlen, El Mostafa Fadaili, Annalisa Romani, Zoran G. Cerovic, Management zone delineation for winegrape selective harvesting based on fluorescence-sensor mapping of grape skin anthocyanins, J. Agric. Food Chem. 66 (23) (2018) 5778–5789.
[37] Fahimeh Ebrahimi Tirtashi, Mehran Moradi, Hossein Tajik, Mehrdad Forough, Parya Ezati, Bambang Kuswandi, Cellulose/chitosan pH-responsive indicator incorporated with carrot anthocyanins for intelligent food packaging, Int. J. Biol. Macromol. 136 (2019) 920–926.
[38] Chandrasekhar Jampani, K.S.M.S. Raghavarao, Process integration for purification and concentration of red cabbage (Brassica oleracea L.) anthocyanins, Sep. Purif. Technol. 141 (2015) 10–16.
[39] Papiya Bigoniya, Kailash Singh, Ulcer protective potential of standardized hesperidin, a citrus flavonoid isolated from Citrus sinensis, Rev. Bras 24 (3) (2014) 330–340.
[40] C.W. Lewis, J.E. Smith, J.G. Anderson, R.I. Freshney, Increased cytotoxicity of food-borne mycotoxins toward human cell lines in vitro via enhanced cytochrome p450 expression using the MTT bioassay, Mycopathologia 148 (2) (2000) 97–102.
[41] Yuxi Lang, Haiyan Gao, Jinlong Tian, Chi Shu, Renyan Sun, Bin Li, Xianjun Meng, Protective effects of α-casein or β-casein on the stability and antioxidant capacity of blueberry anthocyanins and their interaction mechanism, LWT 115 (2019), 108434.
[42] Warangkhana Khaodee, Wanlapa Aeungmaitrepirom, Thawatchai Tuntulani, Effectively simultaneous naked-eye detection of Cu (II), Pb (II), Al (III) and Fe (III) using cyanidin extracted from red cabbage as chelating agent, Spectrochim. Acta A Mol. Biomol. Spectrosc. 126 (2014) 98–104.
[43] Gregory T. Sigurdson, M. Monica Giusti, Bathochromic and hyperchromic effects of aluminum salt complexation by anthocyanins from edible sources for blue color development, J. Agric. Food Chem. 62 (29) (2014) 6955–6965.
[44] Mehrez E. El-Naggar, Mohamed H. El-Newehy, Ali Aldalbahi, Waheed M. Salem, Tawfik A. Khattab, Immobilization of anthocyanin extract from red-cabbage into electrospun polyvinyl alcohol nanofibers for colorimetric selective detection of ferric ions, J. Environ. Chem. Eng. 9 (2) (2021), 105072.
[45] Salhah D. Al-Qahtani, Hanan K. Alzahrani, Omer A. Azher, Zeid O. Owidah, Matokah Abualnaja, Turki M. Habeebullah, Nashwa M. El-Metwaly, Immobilization of anthocyanin-based red-cabbage extract onto cellulose fibers toward environmentally friendly biochromic diagnostic biosensor for recognition of urea, J. Environ. Chem. Eng. 9 (4) (2021), 105493.
[46] Wenting Dang, Libu Manjakkal, William Taube Navaraj, Leandro Lorenzelli, Vincenzo Vinciguerra, Ravinder Dahiya, Stretchable wireless system for sweat pH monitoring, Biosens. Bioelectron. 107 (2018) 192–202.
[47] Adam R. Carr, Yash H. Patel, Charles R. Neff, Sadaf Charkhabi, Nathaniel E. Kallmyer, Hector F. Angus, Nigel F. Reuel, Sweat monitoring beneath garments using passive, wireless resonant sensors interfaced with laser-ablated microfluidics, NPJ Digit. Med. 3 (1) (2020) 1–9.
[48] Annemarijn S.M. Steijlen, Jeroen Bastemeijer, Pim Groen, Kaspar M.B. Jansen, Patrick J. French, Andre Bosssche, A wearable fluidic collection patch and ion chromatography method for sweat electrolyte monitoring during exercise, Anal. Methods 12 (48) (2020) 5885–5892.
[49] Aida Martín, Jayoung Kim, Jonas F. Kurniawan, Juliane R. Sempionatto, Jose R. Moreto, Guangda Tang, Alan S. Campbell, et al., Epidermal microfluidic electrochemical detection system: enhanced sweat sampling and metabolite detection, ACS Sensors 2 (12) (2017) 1860–1868.